Mechanisms for the Interannual Variability in the Tropical Indian Ocean. Part I: The Role of Remote Forcing from the Tropical Pacific

BOHUA HUANG AND J. SHUKLA

Department of Climate Dynamics, College of Science, George Mason University, Fairfax, Virginia, and Center for Ocean–Land–Atmosphere Studies, Institute of Global Environment and Society, Calverton, Maryland

(Manuscript received 14 March 2005, in final form 13 July 2005)

ABSTRACT

A series of experiments are conducted using a coupled ocean–atmosphere general circulation model in regional coupled mode, which permits active air–sea interaction only within the Indian Ocean to the north of 30°S, with sea surface temperatures (SSTs) prescribed over the rest of the world oceans. In this paper, an ensemble of nine simulations has been analyzed with the observed SST anomalies for 1950–98 prescribed over the uncoupled region. The purpose of this study is to determine the major patterns of interannual variability in the tropical Indian Ocean that could be related to the global low-frequency fluctuations and to understand the physical links between the remote forcing and the regional coupled variations.

The ensemble coupled simulations with prescribed SST outside the Indian Ocean are able to reproduce a considerable amount of observed variability in the tropical Indian Ocean during 1950–98. The first EOF modes of the simulated upper-ocean heat content and SST anomalies show structures that are quite consistent with those from the historical upper oceanic temperature and SST analyses. The dominant pattern of response is associated with an oceanic dynamical adjustment of the thermocline depth in the southwestern Indian Ocean. In general, a deepening of the thermocline in the southwest is usually accompanied by the enhanced upwelling and thermocline shoaling centered near the Sumatra coast. Further analysis shows that the leading external forcing is from the El Niño–Southern Oscillation (ENSO), which induces an anomalous fluctuation of the atmospheric anticyclones on both sides of the equator over the Indian Ocean, starting from the evolving stage of an El Niño event in boreal summer. Apart from weakening the Indian monsoon, the surface equatorial easterly anomalies associated with this circulation pattern first induce equatorial and coastal upwelling anomalies near the Sumatra coast from summer to fall, which enhance the equatorial zonal SST gradient and stimulate intense air–sea feedback in the equatorial ocean. Moreover, the persistent anticyclonic wind curl over the southern tropical Indian Ocean, reinforced by the equatorial air–sea coupling, forces substantial thermocline change centered at the thermocline ridge in the southwestern Indian Ocean for seasons. The significant thermocline change has profound and long-lasting influences on the SST fluctuations in the Indian Ocean.

It should be noted that the ENSO forcing is not the only way that this kind of basinwide Indian Ocean fluctuations can be generated. As will be shown in the second part of this study, similar low-frequency fluctuations can also be generated by processes within the Indian and western Pacific region without ENSO influence. The unique feature of the ENSO influence is that, because of the high persistence of the atmospheric remote forcing from boreal summer to winter, the life span of the thermocline anomalies in the southwestern Indian Ocean is generally longer than that generated by regional coupled processes.

1. Introduction

It has long been recognized that fluctuations of the sea surface temperature (SST) in the tropical Indian Ocean are strongly influenced by global-scale climate variations such as the El Niño–Southern Oscillation (ENSO). Statistically, SST increases in the whole Indian Ocean from the late boreal winter of an El Niño year to the next spring, a few months after the peak of the SST anomalies in the eastern Pacific (see, e.g., Pan and Oort 1990; Kawamura 1994; Tourre and White 1995; Lanzante 1996; Nicholson 1997; Klein et al. 1999; Venzke et al. 2000; Allan et al. 2001; Huang and Kinter 2002). These warm SST anomalies then extend into the

Corresponding author address: Bohua Huang, Center for Ocean–Land–Atmosphere Studies, Institute of Global Environment and Society, 4041 Powder Mill Road, #302, Calverton, MD 20705.
E-mail: huangb@cola.iges.org

DOI: 10.1175/JCLI4151.1

northwestern tropical Pacific and persist there well into early summer (Zhang et al. 1999; Wang et al. 2003), which is perhaps the last visible signal of a particular El Niño event. A possible explanation for this wide spread and long-lasting oceanic warming in the Indo–Pacific basin is the cumulative effects of increased solar flux and reduced evaporative heat loss at the sea surface due to the reductions of both cloud cover and surface wind speeds during an El Niño event (e.g., Klein et al. 1999; Venzke et al. 2000). Xie et al. (2002) and Huang and Kinter (2002) also found that the surface warming in the southwestern Indian Ocean at the end of an El Niño year can be caused by an anomalous deepening of the thermocline associated with westward propagating Rossby waves.

Before reaching this basinwide warm state, both the atmosphere and ocean in the Indian basin have already experienced vigorous fluctuations in association with the evolution of an El Niño event. Quite early on during boreal summer of an El Niño year, the eastward shift of major equatorial convection toward the central Pacific forces an anomalous anticyclonic circulation, extending from the western Pacific to the Indian basin (e.g., Lau and Nath 2000, 2003). In response, the Indian monsoon rainfall during June–August is usually below normal in an El Niño year (Rasmusson and Carpenter 1983; Shukla and Paolino 1983; Parthasarathy and Pant 1985; Shukla 1987; Webster and Yang 1992; Webster et al. 1998; Krishnamurthy and Goswami 2000). The weakened monsoon circulation and reduced cloud cover over the northern tropical Indian Ocean increase surface heat flux into the ocean (Shukla 1987), which is consistent with Klein et al.'s explanation for the warming of the Indian Ocean. However, these thermal influences seem most effective in the northern Indian Ocean. Moreover, although this monsoon–ENSO relationship, which is quite significant in historical records up until the 1970s, breaks down during the last two to three decades (e.g., Krishnamurthy and Goswami 2000; Kinter et al. 2002), the pattern of the Indian Ocean warming associated with El Niño events seems to hold steady for the whole period.

On the other hand, ENSO asserts direct dynamic influence on the air–sea feedback within the Indian Ocean near and to the south of the equator. Starting from June and peaking around September, coastal and equatorial upwelling is intensified around the Sumatra coast, driven by surface wind anomalies over the central and eastern Indian Ocean that are likely remotely induced (Hastenrath et al. 1993; Nigam and Shen 1993; Hastenrath 2000). The cooling in the eastern equatorial Indian Ocean prolongs the dry season in Indonesia (Hendon 2003). Within the Indian Ocean, an anomalous zonal SST gradient is established near the equator from late summer to fall, associated with a westward shift of the rainfall and enhanced anomalous easterlies (Saji et al. 1999; Webster et al. 1999; Huang and Kinter 2002; Krishnamurthy and Kirtman 2003). Saji et al. (1999) have pointed out that the rapid growth of this zonal asymmetry or east–west "dipole" is attributable to a positive air–sea feedback involving anomalous SST gradient, surface winds, and precipitation within the Indian Ocean in a way similar to an El Niño development (Bjerknes 1969). The resulting anomalous zonal SST gradient intensifies the "short rain" season over East Africa from October to November (e.g., Hastenrath et al. 1993; Jury et al. 2002; Black et al. 2003; Clark et al. 2003).

The equatorial easterly wind anomalies in the central and eastern Indian Ocean in September and October are accompanied by weaker southeast trade winds. As a result, an anomalous anticyclonic wind curl is established to the south of the equator, which forces significant thermocline deepening in the central part of the southern Indian Ocean around 10°S (e.g., Huang and Kinter 2000, 2001, 2002; Xie et al. 2002; Rao et al. 2002; Gualdi et al. 2003a). The subsurface temperature anomalies then propagate westward and deepen the mean thermocline ridge located in the southwestern Indian Ocean a few months later (Xie et al. 2002; Jury and Huang 2004). Masumoto and Meyers (1998) are among the earliest to point out that this kind of westward propagation in the southwestern Indian Ocean is the Rossby wave signal. Starting from boreal fall, when the thermocline is deepening in the west, the warm SST anomalies in the western tropical Indian Ocean, which were quite mild until then, increase rapidly while the cold SST anomalies in the east start to decay. The SST and thermocline depth anomalies peak simultaneously in the western Indian Ocean during the late winter or early spring (Xie et al. 2002; Huang and Kinter 2002). By this time, warm SST anomalies have spread eastward while the subsurface temperature anomalies persist in the southwest. Since the cold SST anomalies in the eastern Indian Ocean have largely dissipated, the basinwide warm phase described at the beginning of the paper prevails (Huang and Kinter 2002; Shinoda et al. 2004).

Several recent heat budget analyses have shown that the rapid warming of the western Indian Ocean during boreal fall of an El Niño year cannot be explained by the surface heat gain from the local atmosphere (e.g., Klein et al. 1999; Murtugudde et al. 1999; Jury et al. 2002; Shinoda et al. 2004). In fact, both the sea surface heights from recent satellite altimetry measurements (e.g., Chambers et al. 1999) and ocean heat content

based on historical subsurface temperature observations (Huang and Kinter 2002) show a strong coherence between the low frequency fluctuations of the thermocline ridge in the southwestern Indian Ocean and the ENSO cycle. An important result from Xie et al. (2002) is that the SST anomalies over the thermocline dome in the southwestern Indian Ocean display a pronounced westward copropagation with thermocline depth anomalies. This copropagation makes it possible to conclude, from observations, that ENSO-induced ocean Rossby waves are an important mechanism for the SST variability in this region. Xie et al. (2002) further showed that these Rossby waves induce changes in precipitation and surface wind, thereby acquiring a coupled characteristic rather than simply being forced by the atmosphere. Overall, these studies suggest a significant role played by the thermocline dynamics in the coupled variability of the Indian Ocean. The generation of the off-equatorial Rossby waves (Xie et al. 2002; Jury and Huang 2004) makes the air–sea feedback in the Indian Ocean deviate from the classical zonal mode scenario. Huang and Kinter (2002) also speculated that, apart from the anomalous local heat flux, the equatorial zonal gradient and the warming in the western Indian Ocean precondition the subsequent warming over the basin. Overall, ENSO seems to be an effective and persistent remote factor to stimulate the air–sea feedback in the Indian Ocean, both dynamically and thermodynamically. However, it is not yet clear how important the regional air–sea feedback and oceanic dynamics are in shaping the spatial and temporal evolution in response to this external forcing.

On the other hand, even though there is a historical connection between the ENSO cycle and the tropical Indian Ocean fluctuations, it should be noted that ENSO is not a necessary condition for at least some features of the Indian Ocean fluctuation described above to occur. In fact, several intense equatorial Indian Ocean dipole events observed during the past few decades, such as those from the late summer to early winter of 1961, 1967, and 1994, occurred in the years when the eastern Pacific is relatively normal (Saji et al. 1999). A difference between the ENSO and non-ENSO events seems to be that the latter do not have SST anomalies as strong as the ENSO-related events in the mature and decaying phases during late boreal winter and subsequent spring (Huang and Kinter 2002). However, the two kinds of events show considerable similarity in their growth phase during boreal late summer and fall, which suggests that both are likely dominated by the intense air–sea feedback within the Indian Ocean during that phase. It is not clear whether the non-ENSO events are spontaneously generated by air–sea coupling within the Indian Ocean or are triggered by other external sources. Even less is known about the nature of the regional air–sea mode itself. Is it self-sustained with some intrinsic quasi-regularity? Or, is it simply a feedback mechanism in response to other external "triggers"? Recently, Annamalai et al. (2003) have shown that the non-ENSO dipole events share a common precursor of positive SST anomalies in late spring in the western tropical Pacific.

Given this complicated situation, it is certainly useful to know to what extent observed Indian Ocean variations in the past decades can be explained by the external ENSO influences and what other internal and external conditions favor this kind of anomalous development. It is also important to understand how the dynamical air–sea interactions within the Indian Ocean affect the evolution of the Indian Ocean anomalies and the life span of the anomalous events. Similarly, we would like to know how the subsurface oceanic dynamics within the Indian Ocean determine its response to ENSO forcing. Answers to these questions are a prerequisite to understand the predictability of the climate variations in the Indo–Pacific basin. It should also be helpful to design an efficient observational network to monitor the interannual variability in the Indian Ocean and to predict future anomalous events.

We have conducted a series of controlled numerical experiments using a coupled ocean–atmosphere general circulation model (CGCM) to examine some of these issues. In particular, we have used a regional coupling approach, which permits active air–sea interaction only within the Indian Ocean to the north of 30°S while SST is prescribed over the rest of the world oceans. In the first part of this two-part study, we report results from a set of ensemble simulations, which prescribes the observed SST anomalies for the past few decades over the uncoupled domain. The observed SST anomalies should produce realistic atmospheric teleconnections, such as those simulated in an uncoupled atmospheric GCM, while their influences on the air–sea interactions in the Indian Ocean can be diagnosed through the regional coupling. Therefore, this type of simulation should have more realistic ENSO influence on the Indian Ocean than a straightforward global coupled model simulation because current coupled models usually produce weaker ENSO signals than the observed one. Moreover, the spatial and temporal structures of ENSO are usually distorted in these coupled models. Another merit is that the hindcast results are directly verifiable with observational data in the Indian basin.

This paper is structured as follows. The model experiments are briefly described in the next section. The

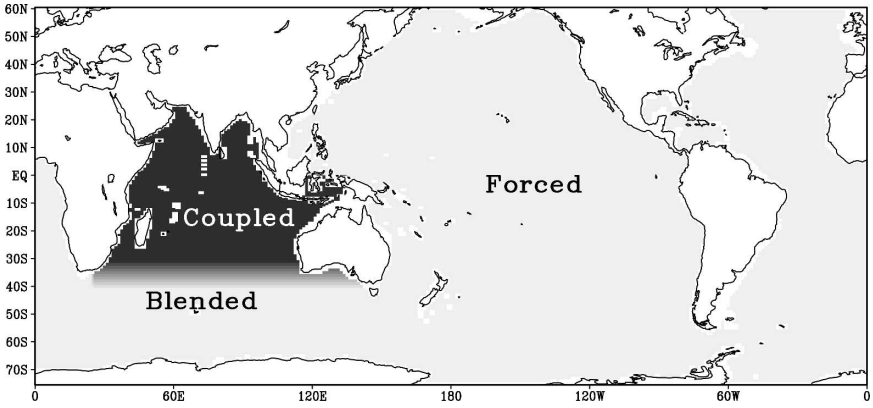

FIG. 1. The regional coupling strategy over the oceanic domain. The fully coupled region is darkly shaded. The oceanic region where the OGCM and the AGCM are forced with data is lightly shaded. For the hindcast experiments, the climatological monthly SST from a long-term global coupled run plus observed SST anomalies are used. The zonal belt over the south Indian Ocean with changing shading is the blending zone.

ensemble mean simulation is verified with observational datasets in section 3. The forced variability of the experiments in the tropical Indian Ocean is examined in section 4. Section 5 summarizes the results of this study and discusses its relevance to our understanding of the variability and predictability in the tropical Indian Ocean. In the second part of this study, we examine an experiment with the climatological SST annual cycle prescribed over the uncoupled ocean. In this experiment, the low-frequency atmospheric signals induced by SST anomalies such as ENSO are suppressed in the model, and the air–sea interactions within the tropical Indian Ocean can operate in a relatively isolated environment.

2. Experiment design

The atmospheric component of the coupled model (referred to as the AGCM hereafter) is a global spectral model using a triangular truncation of the spherical harmonics at wavenumber 42 with 18 σ (terrain following) vertical levels. The oceanic component (the OGCM) is a near global (70°S–65°N) nonlinear quasi-isopycnal model of 14 layers, with a horizontal resolution of 1° latitude $\times$ 1.25° longitude, meridionally increased to 0.5° within 10°S–10°N. Schneider et al. (2001) and Schopf and Loughe (1995) describe the numerical treatment of the dynamics and the parameterization of the subgrid physical processes for the AGCM and OGCM, respectively.

The regional coupling procedure is largely the same as described by Huang (2004) and Huang et al. (2004) for the tropical Atlantic Ocean. In this study, the OGCM and AGCM are fully coupled in the Indian Ocean to the north of 30°S only (Fig. 1, darkly shaded region), where the surface fluxes of heat, freshwater, and momentum at the sea surface simulated by the AGCM are provided to the OGCM at daily intervals;so is the OGCM-produced SST to the AGCM. Outside the coupled oceanic basin (Fig. 1, lightly shaded region) SST and surface wind stress are prescribed for the AGCM and OGCM respectively; that is, in this uncoupled region, the AGCM sees the prescribed SST instead of the one produced by the OGCM. The same is true for the wind stress forcing to the OGCM. A 10°-wide zone in the south Indian Ocean within 30°–40°S is used to blend the coupled and uncoupled portions of the domain, which shows variable shading in Fig. 1.

For the hindcast experiments, the prescribed SST over the uncoupled region to force the AGCM are the monthly SST climatology from a long-term simulation of a global CGCM run plus observed SST anomalies from the U.S. Climate Prediction Center (CPC) SST data for 1950–98 (Smith et al. 1996). The reason for using the CGCM monthly SST climatology is that our preliminary experiments using the total observed SST in the uncoupled region seems to force the center of the annual mean precipitation within the Indian Ocean away from the Sumatra coast.

On the other hand, the uncoupled region of the OGCM is forced by the real-time monthly mean surface wind stress for the hindcast experiments. The stress data are from the National Centers for Environmental Prediction–National Center for Atmospheric Research (NCEP–NCAR) reanalysis for 1950–98 (Kalnay et al. 1996). The net surface heat flux into the OGCM over the uncoupled portion of the global do-

main is given by the AGCM flux plus a relaxation term to the prescribed SST with a rate of 30 W m^{-2} $°C^{-1}$ of the difference between the prescribed and model SST. The freshwater flux is given from the AGCM output without any modification. It should be pointed out here that, although observational data are used as boundary conditions for both OGCM and AGCM in their uncoupled interface, the prescribed SST forcing to the AGCM is much more crucial because it directly induces large-scale atmospheric responses and associated teleconnections. On the other hand, the observational forcing of the OGCM only influences the coupled region indirectly through the meridional transport across 40°S in the south Indian Ocean, as well as the transport by the Indonesian Throughflow. The model in the coupled domain is not sensitive to the prescribed stress data in the uncoupled domain.

To start the hindcast experiments, a 200-yr simulation is first conducted using this regional coupled system with prescribed CGCM SST and NCEP–NCAR wind stress monthly climatologies over the uncoupled oceans (to be referred to as the CLIM experiment). This simulation starts from an instantaneous state of a long coupled run. Then, a total of nine 49-yr (1950–98) hindcast simulations have been conducted. As in Huang (2004), these simulations are initiated from different atmospheric states but identical oceanic states. The differences in the atmospheric component of the initial state should stimulate independent internal variations in the different runs that are not associated with the prescribed boundary forcing outside the Indian Ocean. For this purpose, these nine atmospheric conditions are randomly chosen instantaneous states at 0000 UTC 1 January of different years from the last 100 years of the 200-yr CLIM simulation. On the other hand, all coupled runs start from the same oceanic initial state, which is also derived from the CLIM experiment. The reason for using identical oceanic initial states for these experiments is to avoid the complications associated with the model long-term drift in the deep ocean, which may cause systematic differences among instantaneous oceanic states picked at different periods of the 100-yr run. Our results show that the perturbed atmospheric states are effective in generating significant differences in the upper ocean quickly. A quasi balance between the upper ocean and the atmosphere should be reached within a few months.

The CGCM in global coupled mode simulates the mean state of the SST realistically in the tropical Indian Ocean (Huang and Shukla 2007). Quantitatively, however, the annual mean SST of the CGCM is about 1°C colder than the observations in the Indian Ocean to the north of the equator. The SST errors can be as large as 2°C near the coasts of the Bay of Bengal and the Arabian Sea. The model SST annual cycle is largely in-phase with the observations with somewhat overestimated amplitude in the subtropics. The surface wind stress and 850-hPa winds show the observed monsoon circulation associated with the meridional migration of the precipitation centers. From November to December, however, the belt of the model precipitation centered in the eastern Indian Ocean to the south of the equator extends too much toward the west. During boreal winter, the transition of the surface winds in the eastern Indian Ocean from southeasterly to northwesterly is delayed by about a month in the model. A broader discussion of the climatological state simulated by a CGCM can be found in Gualdi et al. (2003b).

The model climatology from the hindcast experiments is similar to that from the fully coupled model. In the next sections, we will focus on the interannual variability simulated by the hindcasts and point out the possible effects of the model deficiency of the mean state on the simulated interannual variability.

3. Ensemble hindcasts

In validating the ensemble hindcast, we start by comparing the model air–sea anomalies in September–November (SON, similar acronyms for other multimonth intervals) 1997 with the observations. As one of the strongest anomalous events historically in the Indian Ocean, the 1997–98 event has been thoroughly analyzed by many previous studies (e.g., Yu and Rienecker 1999; Webster et al. 1999; Murtugudde et al. 2000; among others). Figures 2a and 2c show the seasonal averaged anomalies of SST, upper-ocean heat content (HC), and surface wind stress from the nine-case ensemble mean hindcast. The HC is defined as the average ocean temperature for the upper 275 m. Its variations can be used here as a measure of the thermocline fluctuations. Figures 2b and 2d show the anomalies of the CPC SST, NCEP–NCAR reanalyzed surface wind stress, and the sea surface height (SSH) from the TOPEX/Poseidon altimetry measurement (Cheney et al. 1994) for the same season.

Both model and observations show warm SST anomalies extending from the African coast near the equator to the Arabian Sea and the Bay of Bengal (Figs. 2a,b). The model and observed surface wind stresses also show a somewhat similar pattern of the equatorial easterly anomalies together with a broad weakening of the southeast trade winds (Figs. 2c,d). Correspondingly, both the model HC (Fig. 2c) and the satellite SSH anomalies (Fig. 2d) indicate a significant shoaling of the thermocline from the Sumatra coast to

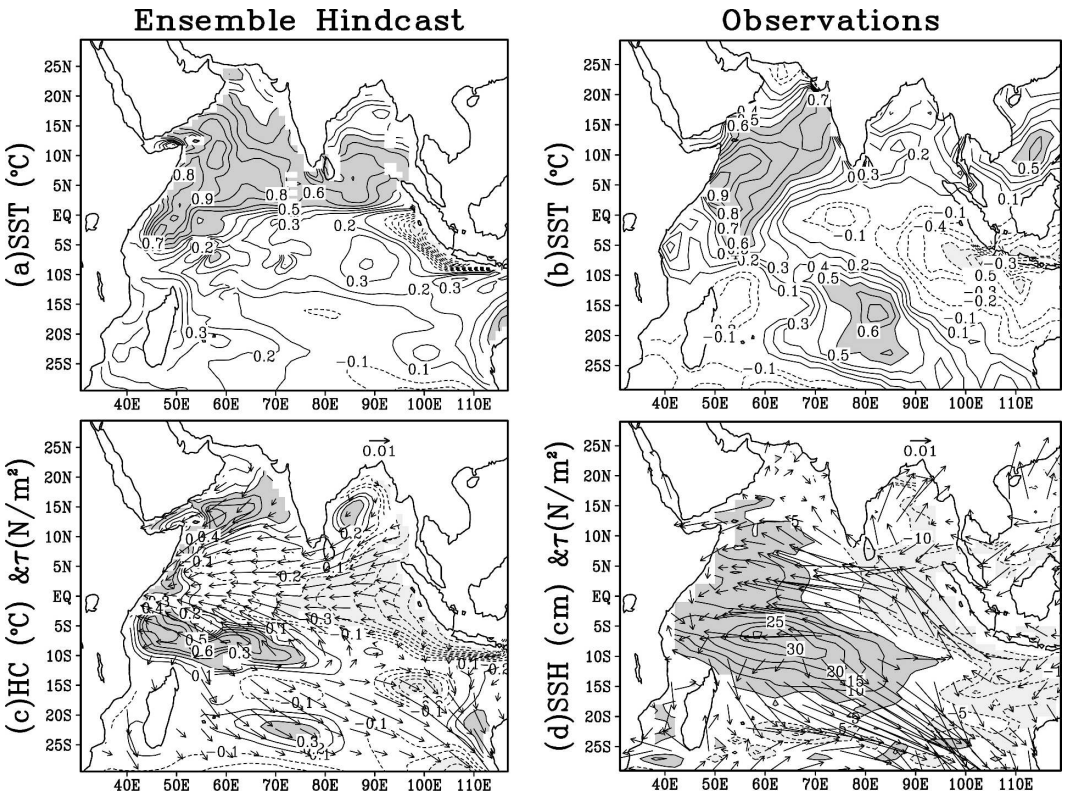

FIG. 2. The ocean–atmosphere anomalies in the tropical Indian Ocean for SON 1997. SST anomalies from (a) the ensemble hindcast and (b) the CPC analysis. The contour interval for SST anomalies is 0.1°C with regions larger than 0.5°C (less than −0.5°C) darkly (lightly) shaded. The vectors show the surface wind stress anomalies for the (c) ensemble hindcast and (d) NCEP–NCAR reanalysis. The unit vector is shown at the upper portion of (a)–(d). The hindcast HC anomalies are shown in (c) with contour interval 0.1°C, and the sea surface height anomalies from the TOPEX/Poseidon altimetry are shown in (d) with contour interval 5 cm. For the HC anomalies, regions with anomalies larger than 0.3°C (less than −0.3°C) are darkly (lightly) shaded. For the sea surface height anomalies, regions with anomalies larger than 5 cm (less than −5 cm) are darkly (lightly) shaded.

the eastern equatorial Indian Ocean, together with a thermocline deepening in the western Indian Ocean centered to the south of the equator and extending northward around the coast. However, the surface cooling associated with the upwelling centered off the Sumatra coast is much weaker in the model compared to the observations (Figs. 2a and 2b) even though the model seems to show broader shoaling of the thermocline in this area (Fig. 2c and 2d). Somewhat surprisingly, the model also misses the observed warm SST anomalies extending southeastward in the southern tropical Indian Ocean, a feature usually attributed to the reduced evaporative heat loss associated with the weakening trades (Yu and Rienecker 1999).

We have looked into each of the nine members of the ensemble in this particular season. It is found that the warm SST anomalies extending from the western coast near the equator to the North Indian Ocean are very robust, appearing in every member. On the other hand, the upwelling signal in the eastern equatorial ocean is more variable, ranging from one very strong cooling case with the cold signals penetrating deeply into the central Indian Ocean to two cases with the anomalous upwelling totally missing. The SST anomalies in the southern central Indian Ocean are also more variable than those in the north. A further examination shows that the HC anomalies from different members are quite consistent in the southwestern ocean and along the western coast. The cold HC anomalies also occur in the equatorial eastern ocean in all but one case. However, their amplitudes fluctuate quite significantly there within the ensemble. Overall, it seems that the SST signals near the Sumatra coast are more strongly influenced by fluctuations independent of the prescribed external forcing. This is also shown in the signal-to-noise ratios for the variance analysis of the SST anomalies to be discussed in the next section.

In spite of some of these shortcomings and uncertainty, it is clear that the hindcast captures many observed features. Figures 3 and 4 compare the first

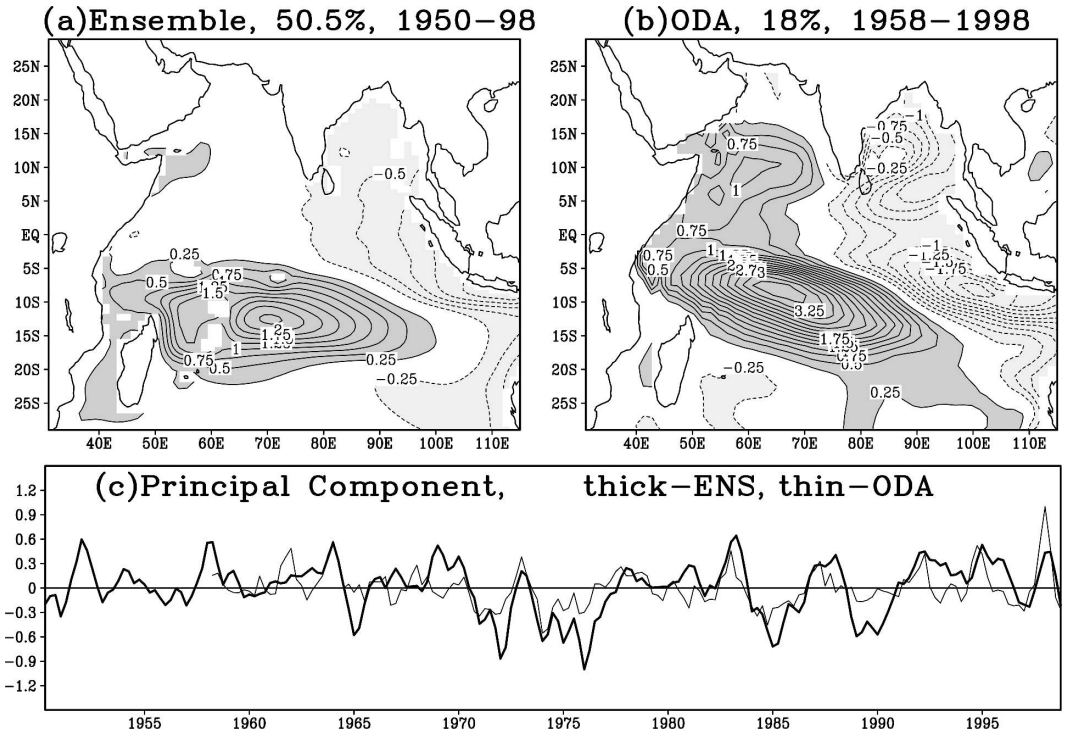

FIG. 3. The first EOF of the seasonal averaged upper-ocean heat content anomalies from the ensemble hindcast and the Center for Ocean–Land–Atmosphere Studies (COLA) ocean data assimilation (ODA) analysis. The spatial patterns of the EOF modes from (a) the hindcast and (b) the ODA analysis. Contour interval is 0.25°C with the zero contour omitted. Regions with anomalies larger than 0.25°C (less than −0.25°C) are darkly (lightly) shaded. (c) Principal components from the ensemble hindcast (thick) and the ODA analysis (thin). The principal components are normalized to have unit maximum magnitude.

modes of the empirical orthogonal functions of the ensemble-mean seasonal averaged model SST and HC anomalies with those derived from the observations based on an ocean data assimilation (ODA) system (Huang et al. 2002; Huang and Kinter 2002). The ODA SST used here is similar to the CPC data used in Fig. 2b in mean state, annual cycle, and interannual variability. For instance, the time series of the averaged SST anomalies in the western equatorial Indian Ocean (10°S–10°N, 50°–70°E) have a correlation coefficient of 0.95 and rms difference of 0.1°C between these two fields. In general, the point-by-point correlations between the ODA and CPC SST anomalies are above 0.7 and their rms differences are below 0.3°C over most of the tropical Indian Ocean (Huang and Kinter 2001).

Since the model and ODA data span different time periods, their EOFs are calculated separately. However, their large-scale structures of the EOF1 for HC anomalies show remarkable similarity. Both the model and ODA HC anomalies demonstrate a leading basin-wide fluctuation with the spatial structure of a weakened thermocline ridge in the southwestern Indian Ocean and a shoaling of the thermocline in the eastern Indian Ocean centered near the Sumatra coast (Figs. 3a and 3b). Somewhat more symmetric with respect to the equator, the observed HC anomalies have corresponding centers in the north although they are weaker than their counterparts in the south. This quasi symmetry is reminiscent of the equatorial oceanic Rossby waves generated by equatorial zonal wind anomalies or the reflection of equatorial Kelvin waves from the eastern coast. The model HC anomalies, however, are more concentrated in the south.

Temporally, the model and ODA principal components of the HC anomalies (Fig. 3c) are significantly correlated during their common period, with a correlation coefficient of 0.61. A visual examination of the two curves shows that many major Indian Ocean "events" have been reproduced, such as the warm episodes in 1968, 1972, 1982, 1986, 1992, and 1997 and the cold episodes in 1971, 1974, and 1984. Admittedly, the major anomalous events in 1961 and 1967 are missed by the hindcast. However, the model does have some success in reproducing the 1994 event. The ensemble simulation also shows several false alarms for both cold and warm events, notably the model cold event in 1965 as

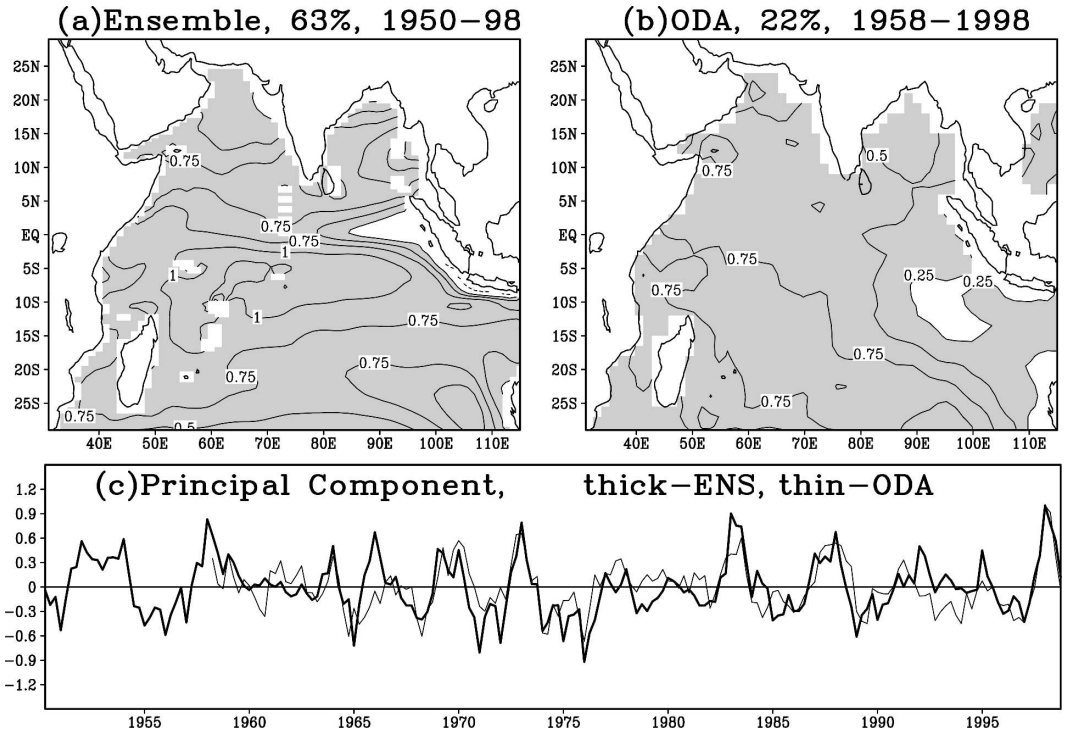

FIG. 4. As in Fig. 3 but for the SST anomalies from the ensemble hindcast and the COLA ODA analysis.

well as the other episodes in the late 1970s and early 1990s (Fig. 3c).

On the other hand, although the basinwide warming is captured by the hindcast SST anomalies, the model SST EOF pattern (Fig. 4a) is distorted in comparison with the observations (Fig. 4b), mainly in missing the broad warm anomalies in the southern tropical Indian Ocean, in the same way as the simulated 1997 event. This systematic discrepancy may be related to the model deficiency that the deepening of the southern thermocline is initiated farther to the west than in the observations, as will become clearer in the next section. On the other hand, the correlation coefficient of the principal components of the model and ODA SST anomalies is 0.67 and the two time series (Fig. 4c) basically present the same relationship as shown in the principal components of the HC anomalies.

Since no observational information for 1950–98 is provided to the model within the Indian Ocean basin, the remarkable resemblance between the observations and the model ensemble hindcast, presented in Figs. 2, 3, and 4, must be due to factors outside the coupled region, where the observational information is provided through the prescribed SST anomalies for 1950–98. Our results suggest that the forcings outside the Indian Ocean provide substantial influence over the basinwide circulation pattern within the tropical Indian Ocean and the predictability of its interannual variability. The sources of these external forcings and the possible physical processes through which these external sources affect the Indian Ocean will be discussed in the next section.

4. The forced pattern

a. General characteristics

For an ensemble of simulations under the same boundary condition but from different initial conditions, the total variance of a variable can be decomposed into a forced component mainly associated with the variance of its ensemble mean and an internal component defined as the sum of the variances of each run's deviation from the ensemble mean (Rowell et al. 1995). Figure 5 shows the forced and internal variances as well as their ratios for the seasonal mean SST and HC anomalies. These ratios give a measure of the potential predictability (Rowell 1998). It is clear that the forced signals are dominant in the southwestern Indian Ocean for both SST and HC anomalies and for the SST anomalies in the northern Indian Ocean between 5° and 15°N. Near the upwelling zone off the Sumatran coast, the forced and internal signals are of nearly the same magnitude for the HC anomalies (Fig. 5f) while the internal signals are more active in the SST anoma-

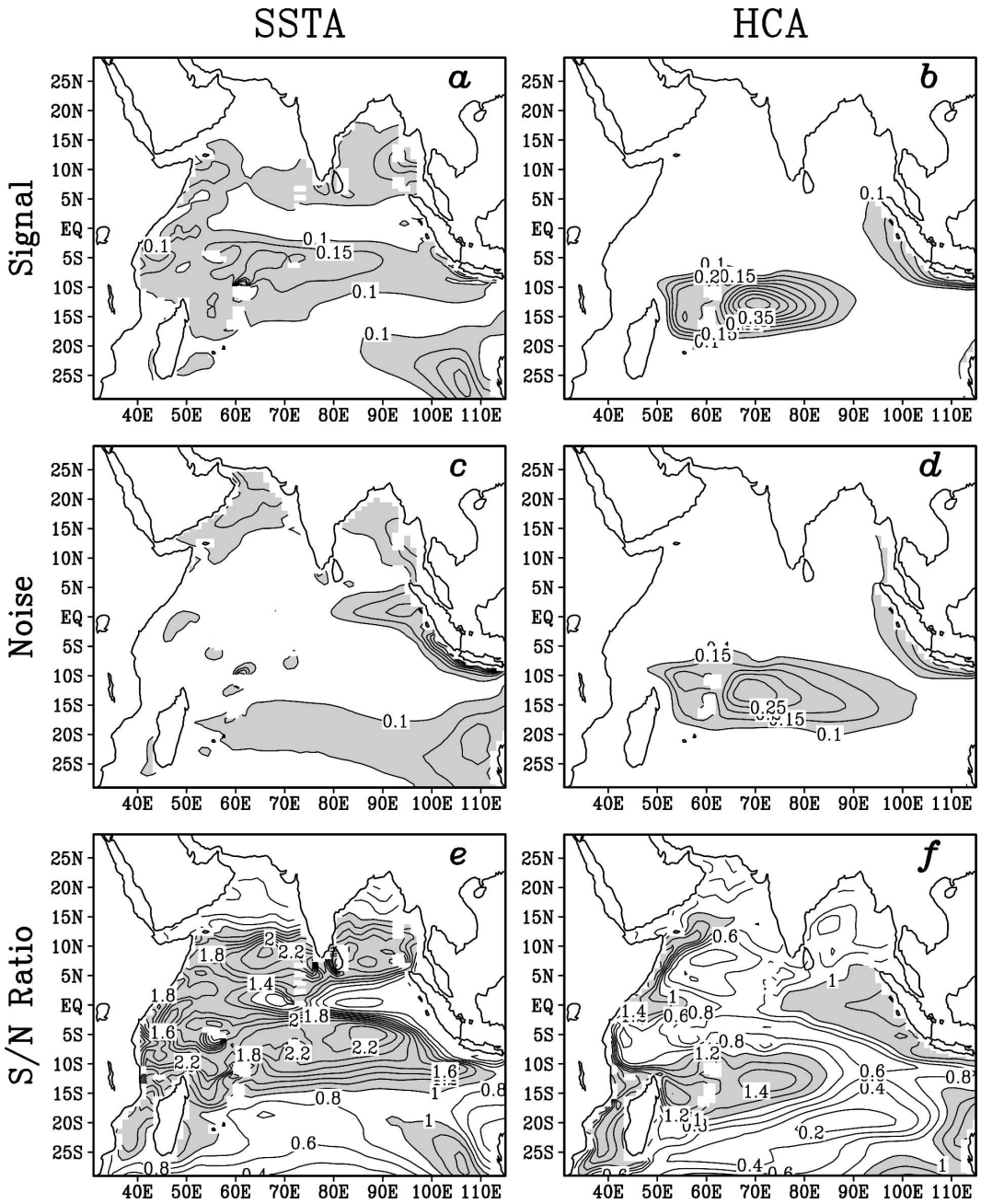

FIG. 5. A variance analysis of the seasonally averaged (left) SST and (right) HC anomalies from the nine 1950–98 simulations: (a),(b) variances of the forced signals; (c),(d) noise variances; and (e),(f) ratios between the signal and noise as demonstrated by (a)–(d). Contour intervals are 0.05 $(°C)^2$ for the variance maps and 0.1 for the ratio maps. For the variance maps, regions larger than 0.01 $(°C)^2$ are shaded. For the ratio maps, regions larger than 1 are shaded.

lies (Fig. 5e). These are consistent with the larger intraensemble SST fluctuations there in the fall season of 1997 described in the last section. Moreover, the forced patterns are largely similar to what we derived from the leading EOF modes of the SST and HC anomalies using the ensemble mean data. Therefore, unlike the tropical Atlantic Ocean, where the regional and random air–sea signals are relatively strong and more sophisticated statistical techniques are required to extract the remotely forced low-frequency signals (Huang 2004), the forced modes here seem to be adequately derived by the leading EOF modes of the ensemble

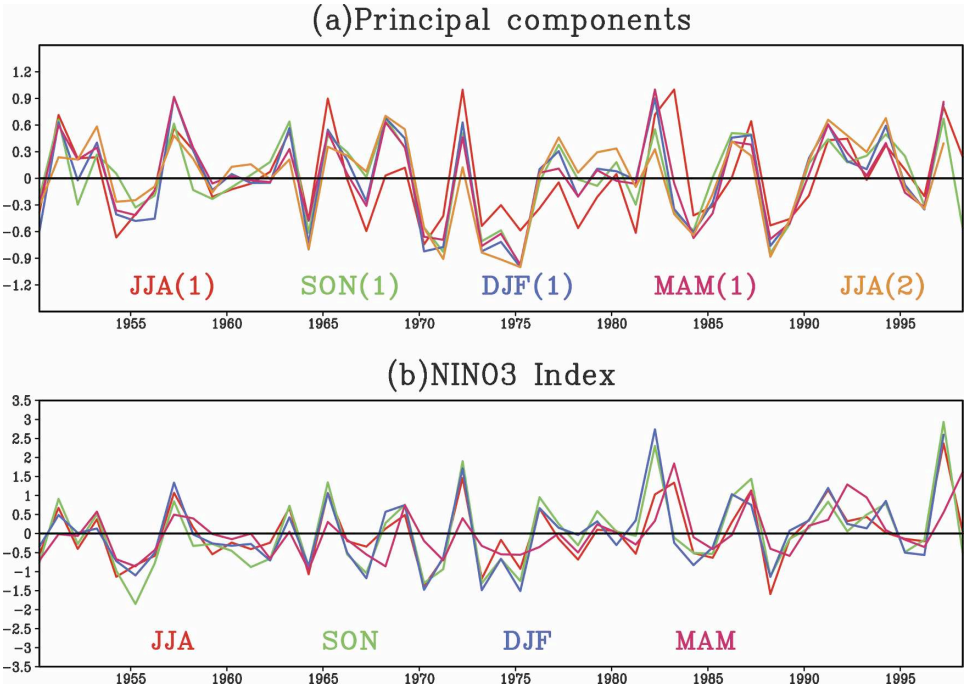

FIG. 6. (a) PCs of the first multivariable EOF modes for JJA (red), SON (green), DJF (blue), and MAM (purple), and the second multivariable EOF mode for JJA (orange). All PCs are normalized to have the unit maximum magnitude. In the plot, the first PC of MAM and the second PC of JJA are shifted forward by 1 yr to show their lagged consistency with the other time series. (b) Niño-3 indices for the four seasons. The color code for each season is the same as the corresponding first PCs in (a). Unit of the Niño-3 index is °C. There is no 1-yr shift of the MAM Niño-3 index.

means of the nine cases. This is mainly because the internal noise is modest in the Indian Ocean and the regional air–sea interactions are more tightly coupled with the influences of the global-scale low-frequency fluctuations.

To delineate the evolution of the remotely forced variability in the tropical Indian Ocean, we have analyzed the leading modes of the multivariable EOF of the seasonal averaged anomalies of the SST, HC, wind stress, and the net surface heat flux from 1950 to 1998 using the ensemble mean data. The procedure of calculation follows Nigam and Shen (1993). Figure 6a shows the principal components (PCs) of the first multivariable EOF modes for JJA (red), SON (green), DJF (blue), and MAM (purple) and the second multivariable EOF mode for JJA (orange). In the figure, the first PC of MAM (purple) and the second PC of JJA (green) are shifted forward by one year. With this shift, it is clear that these five time series are closely lined up with each other, which demonstrates a lagged consistency or persistence of the leading signals from season to season for five seasons.

In fact, the principal components of the first EOF modes are highly correlated from one season to another following the sequence of June–August to the March–May of the subsequent year. The correlation coefficients are around 0.9 from SON to the next MAM. Although the JJA–SON correlation is somewhat lower (0.69), it is still highly significant statistically. On the other hand, although the first PCs from MAM to the following JJA are nearly uncorrelated (0.13), the correlation coefficient between the PC of the first MAM multivariable EOF and that of the second JJA mode is 0.87. Moreover, the lagged correlation between the PCs of the first and the second multivariable EOF modes in JJA is 0.59, with the former leading the latter by one year, even though their simultaneous correlation is zero by definition, which is verifiable with data. Overall, this correlation pattern suggests a nearly continuous process that initiates in the JJA and evolves until the same season of the subsequent year.

This evolving process is highly correlated with the prescribed ENSO cycle in the tropical Pacific. Figure 6b shows the Niño-3 indices for different seasons with the same color code as the first PCs in Fig. 6a for different seasons. The Niño-3 index is defined as the area-averaged SST anomalies from the eastern to central equatorial Pacific (5°N–5°S, 90°–140°W) and character-

TABLE 1. Correlation coefficients between the principal components of the leading multivariable EOF modes in the tropical Indian Ocean for different seasons and the observed Niño-3 index in the same season (lag = 0) and one season (lag = 1) or two seasons (lag = 2) before. Bold values in the table represent correlations that pass the 99% significance test.

Lag	JJA EOF1	SON EOF1	DJF EOF1	MAM EOF1	JJA EOF2
0	**0.86**	**0.75**	**0.87**	**0.50**	−0.16
1	**0.69**	**0.70**	**0.85**	**0.89**	**0.47**
2	0.22	0.41	**0.80**	**0.84**	**0.69**

izes the ENSO variability. A visual examination clearly shows the correspondence between the PCs and the Niño-3 indices. Table 1 quantifies this relationship with the correlation coefficients of the PCs with the seasonal Niño-3 indices. The correlations are calculated simultaneously, as well as with the Niño-3 index leading for one or two seasons, respectively. The results establish a clear relationship of ENSO forcing the Indian Ocean variability. In fact, from boreal summer (JJA) to fall (SON), the simultaneous PC–ENSO correlations are largest, with high correlations when ENSO leads for one season. In DJF, the simultaneous correlation is the highest and the significant lagged high correlations between the PC and Niño-3 extend back to two seasons. On the other hand, both the PC for MAM and the second PC for JJA have the highest correlation with the previous DJF Niño-3 while the correlations with the simultaneous Niño-3 are much weaker or even insignificant statistically. A possible explanation for this correlation pattern shown in Table 1 is that ENSO starts to influence the Indian Ocean fluctuations in boreal spring while the strongest influences are from summer to the subsequent winter. By the next spring, the direct ENSO forcing has been weakened. However, the persistence within the Indian Ocean and the processes internal to the Indian Ocean still carry the signal forward until the subsequent summer.

b. Spatial–temporal evolution

The features of the time series of the five multivariable EOF modes discussed above seem to allow us to view their spatial patterns in a sequence of the first EOF modes from JJA to MAM characterizing the forced anomalous evolution from the boreal summer of a typical anomalous year to the subsequent spring, while the second EOF mode of JJA characterizes the final stage of the evolution in the summer of the second year. This characterization can be justified by its consistency with the composites of major El Niño and La Niña years during this 49-yr period.

Figure 7 shows the spatial patterns of the first multivariable EOF mode for JJA for HC, SST, wind stress, and net surface heat flux anomalies. The surface wind stress shows east to northeast wind anomalies extending from the Bay of Bengal and the Arabian Sea to the African coast across the equator (Fig. 7c), which indicates a weakening of the Indian summer monsoon. Associated with the weakened monsoon winds are the anomalous easterlies over the central and eastern equatorial Indian Ocean, as well as the weakened southeast trade winds around 15° to 25°S. The weak monsoon seems to induce anomalous surface heat flux into most of the northern tropical Indian Ocean, especially within the Arabian Sea and near the coast of Sumatra around 5°N (Fig. 7d). Moreover, the weak southeast trade winds also induce anomalous heat into the ocean to the south of 15°S. As a result, SST is warmed in the Indian Ocean to the north of the equator and in the southwestern part of the ocean (Fig. 7b).

The maximum temperature rise of 1°C, however, is near the western coast near 5°–10°N, which is more likely associated with the weakened upwelling and the slightly deepened thermocline there (Fig. 7a) because of the anomalous coastal winds. On the other hand, the anomalous equatorial winds generate shoaling of the thermocline around the Sumatra coast (Fig. 7a) that, in particular, is responsible for the surface cooling within the limited region off the Sumatra coast between 5° and 10°S (Fig. 7b). The cooling is apparently dynamically driven because the local surface heat flux tends to damp it out (Fig. 7d). Finally, a broad band of surface heat loss is located in the southern Indian Ocean between 15°S and the equator (Fig. 7d), which, curiously, is centered on a relatively calm zone of weak wind anomalies (Fig. 7c). This heat loss seems to be countered by a mild tendency of the thermocline deepening in the southern open ocean.

By September–November (Fig. 8), the easterly wind anomalies have enhanced significantly around the equator, as do the southeast trade wind anomalies farther to the south (Fig. 8c). As a result, a strong anticyclonic wind shear is established over the southern tropical Indian Ocean, centered within 10°–15°S. This wind curl induces significant deepening of the thermocline to the south of the equator, centered at 10°S, 70°E (Fig. 8a). The westward extension of the HC anomalies is probably a sign of the Rossby wave propagation, as shown by Xie et al. (2002). At the same time, the strong equatorial winds continue to induce coastal and equatorial upwelling and shoaling of the thermocline in the east. The deepening of the thermocline in the southwest and the equatorial and coastal shoaling in the east characterize the basinwide pattern of the HC anoma-

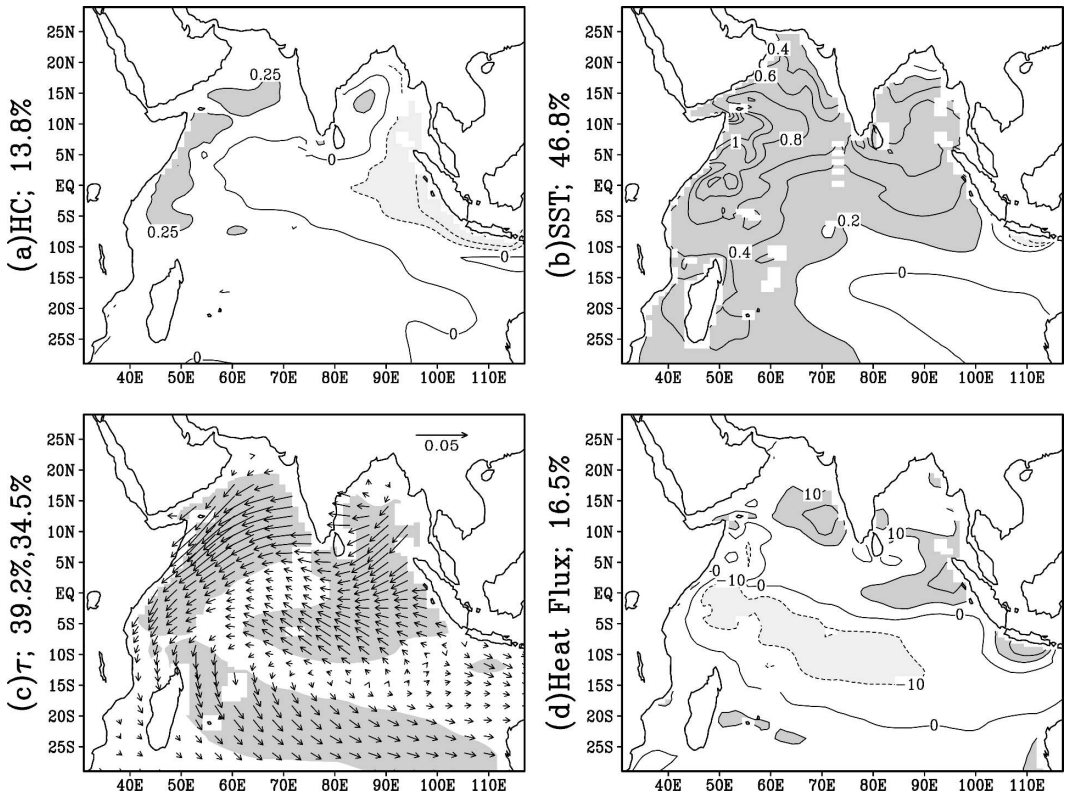

FIG. 7. The spatial patterns of the first multivariable EOF mode for JJA for (a) HC, (b) SST, (c) wind stress, and (d) net surface heat flux anomalies. Contour intervals are 0.25°C for HC in (a), 0.2°C for SST in (b), and 10 W m^{-2} for the heat flux in (d). The vector of 0.05 N m^{-2} is shown on the upper-right corner in (c) for surface wind stress. The dark (light) shadings in (a),(c),(d) show HC anomalies larger than 0.25°C (less than −0.25°C), SST anomalies larger than 0.2°C (less than −0.2°C), and surface heat flux anomalies larger than 10 W m^{-2} (less than −10 W m^{-2}), respectively. The shading in (c) shows the areas of wind stress magnitude larger than 0.01 N m^{-2}. The percentage explained by this mode to the total combined variance is 30.0%. The percentage of variance explained for each variable by its corresponding pattern is given on the lhs of (a)–(d).

lies, as shown in Fig. 3 for the observations and the model hindcast.

The surface cooling off the Sumatra coast is enhanced and slightly expanded, which, together with the warm SST anomalies farther to the east, forms an anomalous zonal SST gradient or the dipole pattern (Fig. 8b), as described by Saji et al. (1999) and Webster et al. (1999). At this season, the surface heat flux becomes a damping term over most of the Indian Ocean except for the Bay of Bengal and over some regions of the subtropical south Indian Ocean (Fig. 8d). Around 15°S a belt of cold SST anomalies extends westward (Fig. 8b), which is probably a delayed response to the surface heat loss in the last season around this area (Fig. 7d). Its geographic location links it potentially to the fluctuations of the transport by the Indonesian Throughflow. This possibility has yet to be further explored.

The easterlies have shifted farther southward away from the equator by December–February, probably because of the stronger zonal SST gradient there. The anticyclonic wind curls are sustained over the southern Indian Ocean and may even be enhanced (Fig. 9c). Correspondingly, the basinwide HC pattern is also enhanced in both the southwestern and eastern centers, which are all shifted slightly southward (Fig. 9a). Around these two centers, the subsurface temperature anomalies seem to exert significant influence on the SST. For instance, the warming between the equator and 15°S in DJF is generally opposed by the surface cooling during the past two seasons (Figs. 8d and 9d) and has to be accounted for by the thermocline influence. In particular, the closeness of the warm SST center around 5°–10°S, 60°–70°E in DJF (Fig. 9b) with the center of the positive HC anomalies in both SON and DJF reinforces the proposed relationship. This is consistent with Xie et al.'s (2002) findings based on the observations. The surface warming in the Indian Ocean

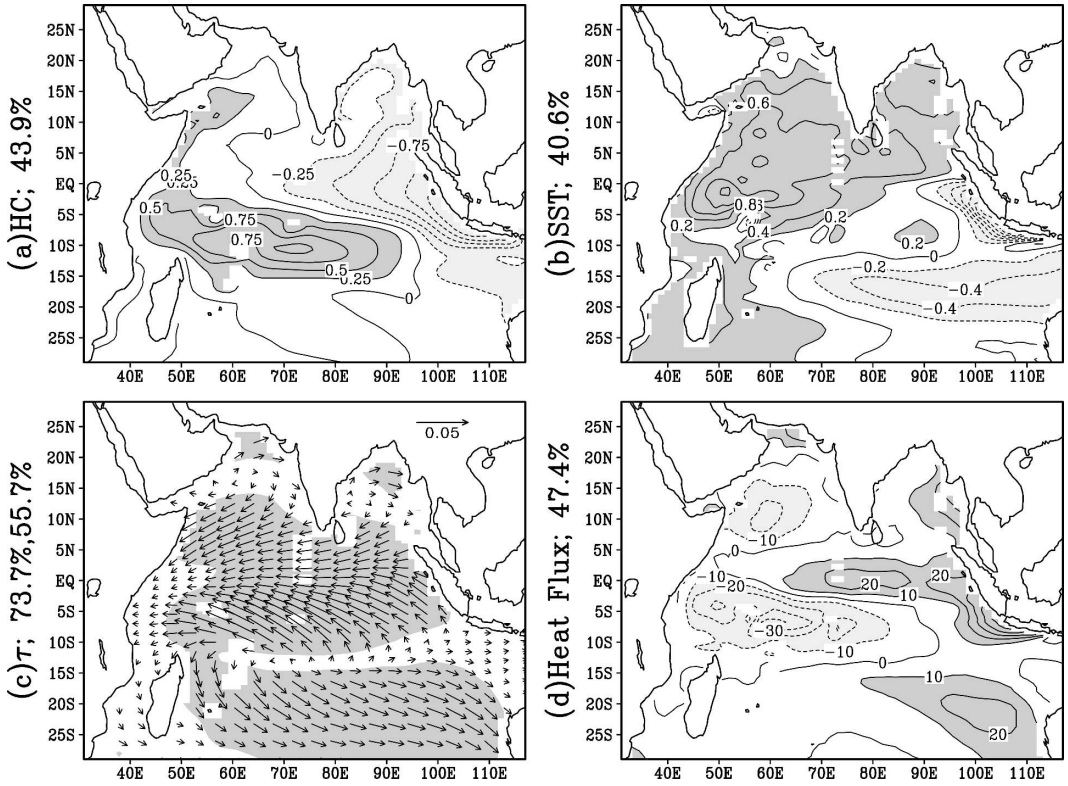

FIG. 8. As in Fig. 7 but for SON with explained percentage of total combined variance at 51.9%.

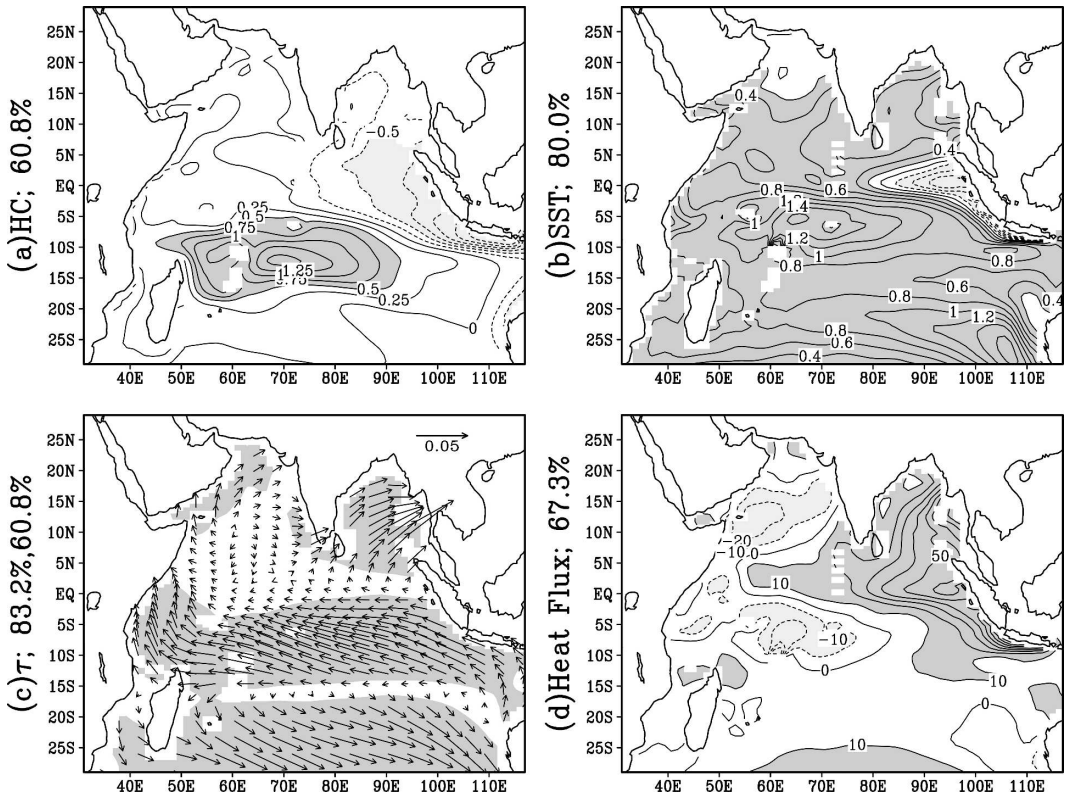

FIG. 9. As in Fig. 7 but for DJF with explained percentage of total combined variance at 70.4%.

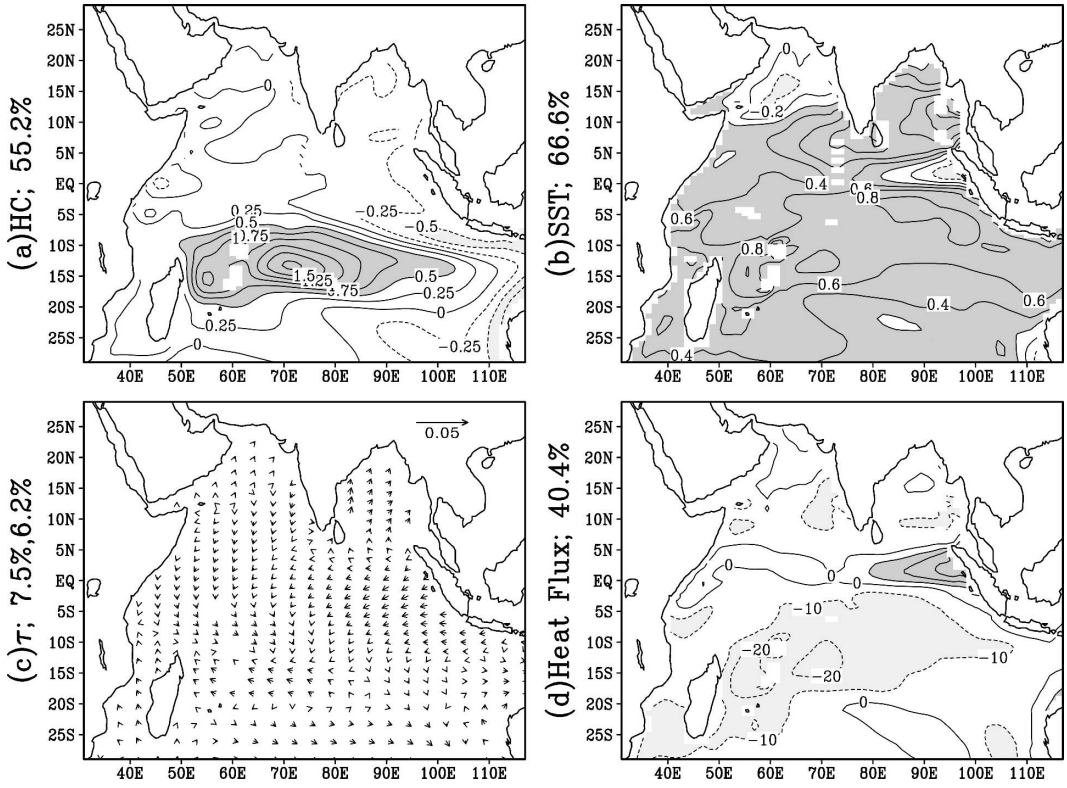

FIG. 10. As in Fig. 7 but for MAM with explained percentage of total combined variance at 36.0%.

to the south of 15°S, however, is probably attributable to the anomalous surface heat flux since SON. In particular, the anomalous SST center to the west of Australia (Fig. 9b) corresponds to the center of the net heat flux into the ocean in SON (Fig. 8d). On the other hand, the more persistent cold signals off the Sumatra coast in this and the next seasons are somewhat different from the observations, which show a quick decay of the cooling in the east during the late boreal winter and early spring (e.g., Huang and Kinter 2002). This model discrepancy is probably related to its delayed climatological wind transition from the southeasterly to the northwesterly in the eastern Indian Ocean. Hendon (2003) and Shinoda et al. (2004) have shown the seasonal transition as a major factor to damp out the ENSO-induced SST anomalies in this region. Another possibility is that the model does not generate strong enough equatorial downwelling Kelvin wave signals in the west to propagate to the eastern coast and suppress the local cooling there at this season (Huang and Kinter 2001; Rao et al. 2002).

It is interesting that the anomalous anticyclonic winds have largely disappeared over the tropical Indian Ocean in the subsequent MAM season (Fig. 10c), which probably signals the end of the direct ENSO forcing. However, the major HC anomalies to the south of the equator are persistent (Fig. 10a). The warm signals are also persistent at the sea surface to the south of the equator and around the Bay of Bengal (Fig. 10b) against the damping effects of the surface heat flux over most of the Indian Ocean (Fig. 10d). We would like to emphasize that the warm SST anomalies in the Bay of Bengal have been thermally forced by anomalous surface heat flux into the ocean from JJA to DJF (Figs. 7d–9d). After the local heat flux becomes a damping there since MAM (Figs. 10d and 11d), these SST anomalies are weakened significantly in the next season (Fig. 11b).

On the other hand, the development of the HC–SST anomalies in the southwest is generally against the local surface heat flux anomalies throughout these seasons. It is these oceanic anomalies that seem to persist longer. In the subsequent JJA season, while small and insignificant SST anomalies scatter around in other parts of the basin, large anomalies of SST and HC are found to persist in the southwestern Indian Ocean (Figs. 11a and 11b) against local heat flux damping (Fig. 11d). Moreover, winds seem to be reversed from their direction of the previous summer over the southern tropical Indian Ocean (cf. Figs. 7c and 11c). Both features are probably associated with the thermocline deepening in preceding months. The possibility of strong oceanic dynamical in-

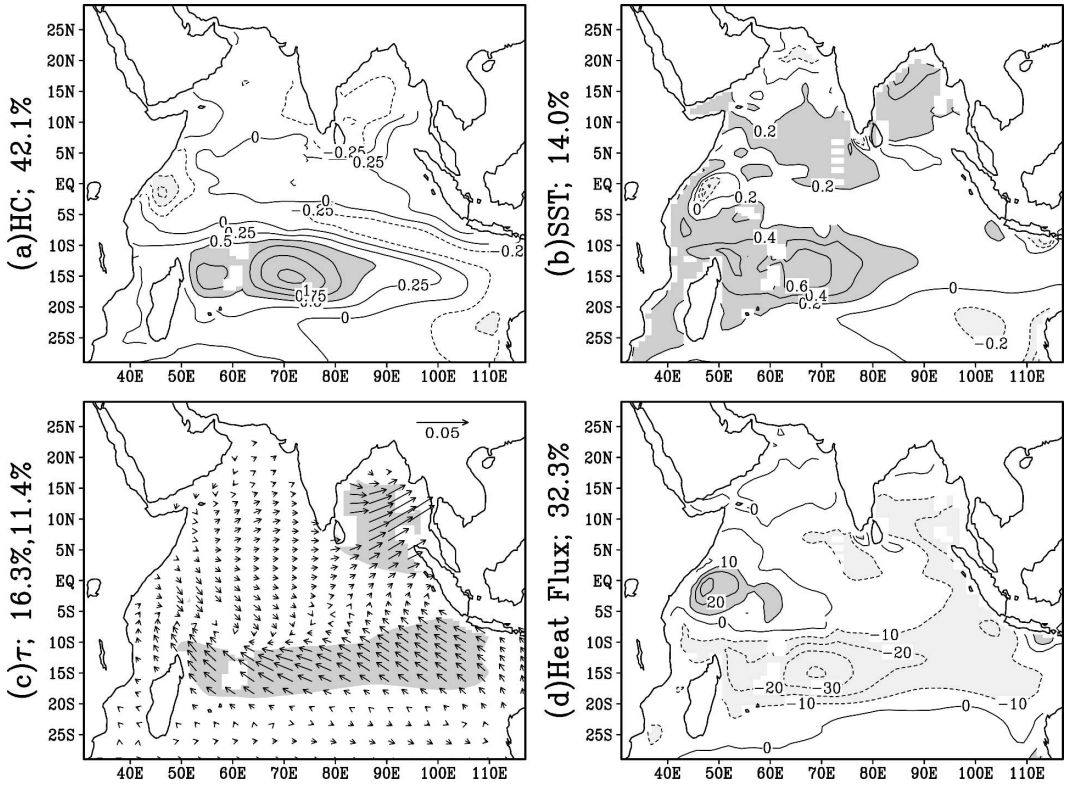

FIG. 11. As in Fig. 7 but for the second multivariable EOF mode for JJA with explained percentage of total combined variance at 23.5%.

fluence in the southwestern Indian Ocean has been suggested by previous studies (Xie et al. 2002; Huang and Kinter 2002; Shinoda et al. 2004). Using observational data, Xie et al. (2002) have shown this long persistence into summer of copropagating anomalies from the thermocline to the surface (their Fig. 11). They also observed a cyclonic anomalous surface circulation over the SST anomalies in the southwestern Indian Ocean as a regional atmospheric response, a feature also discernible in Fig. 11c to some degree. A new development in this season is that positive HC anomalies appear near the Sumatra coast and most of the equatorial ocean (Fig. 11a), which implies that at least part of the southwestern warm HC signals have penetrated into the equatorial waveguide and propagated eastward as the equatorial Kelvin wave to suppress the thermocline there. This propagation, once started, should be quite fast and cannot be resolved by the seasonal averaged data.

c. Large-scale atmospheric pattern

The connection of this regional evolution with the remote ENSO forcing can be seen in Figs. 12 and 13. The former shows the regression patterns of the seasonal averaged precipitation anomalies in the Indo–Pacific basin for JJA, SON, and DJF with respect to the PC of the first multivariable EOF mode in SON (green curve in Fig. 6a). The latter shows the corresponding regression patterns for the sea level pressure (SLP) and the 850-hPa wind. In the Pacific, the patterns of the precipitation, sea level pressure, and 850-hPa wind anomalies clearly show the development of an El Niño event from boreal summer to winter, which includes a gradual eastward shift of precipitation, a SLP reduction in the central and eastern Pacific, and westerly wind anomalies over the western and central equatorial Pacific. It is interesting to note that the positive precipitation anomalies first appear around 10°N, 160°E over the tropical western Pacific in JJA (Fig. 12a) before shifting southeastward during the next two seasons to the equatorial central Pacific around 150°W (Fig. 12c). This summer precipitation center corresponds to a northwestward extension of the low SLP anomalies and the establishment of a local cyclonic circulation extending as far west as the Asian continent (Fig. 13a).

Associated with this fluctuation in the Pacific, SLP increases at two centers over the Indian Ocean basin near 15°S and 15°N (Fig. 13a). The low-level winds show anticyclonic circulations around these two centers

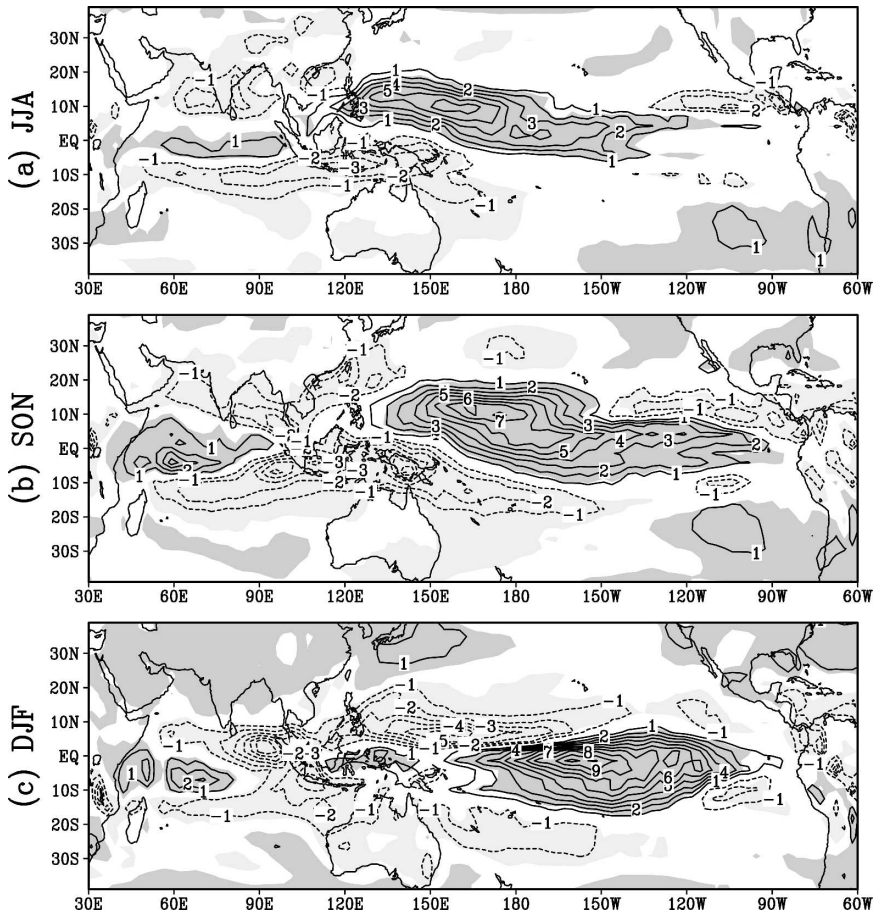

FIG. 12. Regression coefficients of the PC of the first SON multivariable EOF mode on the seasonal averaged precipitation anomalies in (a) JJA, (b) SON, and (c) DJF. Contour interval of the precipitation is 1 mm day^{-1} with zero line omitted. The regions corresponding to the 99% significance level are shaded.

with anomalous easterlies prevailing over the equator. Correspondingly, precipitation is reduced over the South Asian continent and the surrounding seas and over the southern Indian Ocean between 10° and 20°S (Fig. 12a). During the next season, both anticyclonic centers are elongated zonally and enhanced (Fig. 13b). The precipitation also shows an east–west dipole structure near the equator (Fig. 12b), corresponding to the SST dipole in this season. At the same time, the precipitation is further reduced along a belt extending from the Sumatra coast toward Madagascar. By DJF, while the northern anticyclone is weakened, the southern one is further enhanced, together with a northeastward intrusion of the high SLP anomalies into the western tropical Pacific where the SLP has been anomalously low in the previous JJA (Fig. 13c). The SLP pattern corresponds to a precipitation reduction near Australia and the tropical western Pacific (Fig. 12c). Over the southwestern Indian Ocean, the model shows positive rainfall anomalies in SON and DJF (Figs. 12b and 12c), where the positive HC and SST anomalies have been large. Annamalai et al. (2005) have shown that these rainfall anomalies are forced by Rossby wave–induced positive SST anomalies. In the following seasons, atmospheric anomalies such as the anomalous cyclonic wind circulation (Fig. 11c) are likely to be associated with the persistent HC and SST anomalies. Therefore, ENSO-forced anomalies in the Indian Ocean are possibly influenced by such regional air–sea feedback.

Overall, the ENSO influence is to establish anomalous high surface pressure over the tropical Indian Ocean when the eastern Pacific is warmed up. This pattern may be explained by anomalous diabatic heating over the marine continent associated with the ENSO-induced precipitation shift. In response, the tropical Indian Ocean experiences a significant ocean–atmosphere adjustment. The wind curl–induced ther-

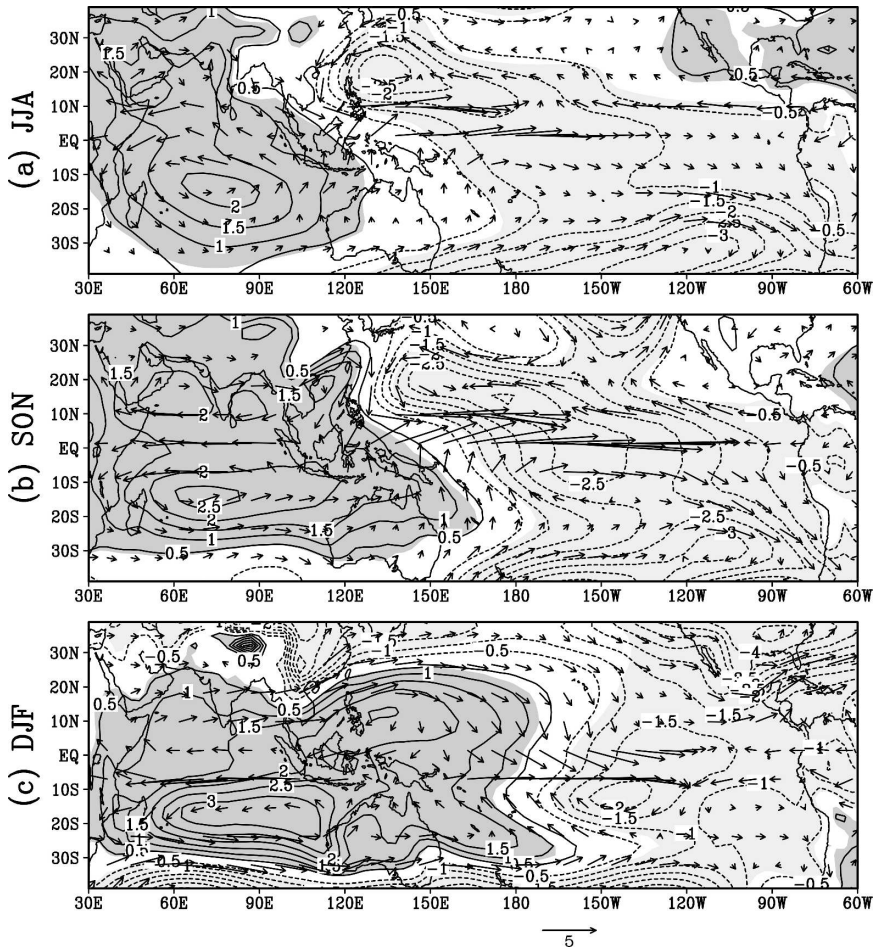

FIG. 13. As in Fig. 12 but on the seasonal averaged sea level pressure and 850-hPa wind anomalies. Contour interval of the sea level pressure is 0.5 hPa with zero line omitted; scale of wind vector of 5 m s^{-1} shown at the bottom of the figure. Shading shows regions corresponding to the 99% significance level for the sea level pressure anomalies.

mocline change in the southwestern part of the ocean provides long-lasting influence over the SST and the atmospheric circulation over this region. In particular, the longer persistence of the southern branch of the anticyclonic centers may be attributable to the intensive oceanic feedback.

5. Summary

A series of experiments was conducted using a coupled ocean–atmosphere general circulation model to examine the mechanisms of the interannual variability in the tropical Indian Ocean. To study the influence of the regional air–sea interactions and the remote forcing, the model is integrated in regional coupled mode, which permits active air–sea interaction only within the Indian Ocean to the north of 30°S, with SST prescribed over the rest of the world oceans. In this paper, we analyzed an ensemble of nine simulations with the observed SST anomalies for 1950–98 prescribed over the uncoupled region. The major purpose of this study is to extract the major patterns in the tropical Indian Ocean that are directly linked to the global low-frequency fluctuations and to understand the physical link between remote sources and regional variations. Another purpose of this study is to identify which observational signals can be categorized as directly related to the remote forcing outside the Indian Ocean basin during this period.

Our results show that a considerable amount of observed variability in the tropical Indian Ocean during 1950–98 can be reproduced by the ensemble coupled hindcast. The first EOF modes of the upper-ocean heat content and SST anomalies from the coupled hindcast

show structures consistent with those of the historical oceanic temperature and SST analysis. The dominant pattern of response is associated with an oceanic dynamical adjustment with the thermocline deepening in the southwestern Indian Ocean, which is generally accompanied by the enhanced upwelling and thermocline shoaling centered near the Sumatra coast. Further analysis shows that the leading external forcing is from the El Niño–Southern Oscillation (ENSO), which in its warm phase induces an anomalous fluctuation of the atmospheric anticyclones on both sides of the equator over the Indian Ocean during its evolving stage in boreal summer. The surface wind anomalies first induce upwelling anomalies near the Sumatra coast, which enhance the equatorial zonal SST gradient and stimulate intense air–sea feedback in the equatorial ocean. Moreover, the anticyclonic wind curls over the southern tropical Indian Ocean, reinforced by the equatorial air–sea coupling, also force a substantial thermocline change centered at the thermocline ridge in the southwestern Indian Ocean. The significant thermocline change has profound and long-lasting influences on the SST fluctuations in the Indian Ocean.

These model results are largely consistent with those derived by Huang and Kinter (2002) from the observations based on the ODA analysis for 1958–98. In particular, the seasonality of the fluctuation of the thermocline in the southwestern Indian Ocean and its relationship with the ENSO cycle are qualitatively similar between the model and the observations. As mentioned before, previous observational studies by Xie et al. (2002) and Huang and Kinter (2002) have shown the westward copropagation of the SST and thermocline depth anomalies as Rossby wave signals that are quite prominent in the southwestern Indian Ocean (Masumoto and Meyers 1998). Xie et al. (2002) have emphasized the influences of these oceanic signals on the precipitation and surface winds. A major discrepancy between the model and the observed HC variations, however, is the weaker oceanic wave characteristics in the model in comparison with the observations. In the observations, the oceanic anomalies are generated in the central Indian Ocean by the equatorial easterly anomalies and the anticyclonic wind curls farther to the south, which clearly propagate westward during the next season as Rossby waves and then persist in the southwestern Indian Ocean (Huang and Kinter 2002; Xie et al. 2002; Jury and Huang 2004). In the model, however, the subsurface anomalies are usually generated in boreal fall farther to the west of the observed position, which then only extend westward and shift slightly southward, although this westward extension may be explained as a sign of wave propagation. A possible explanation of this discrepancy is that, in the model, the El Niño forced anticyclone in the southern tropical Indian Ocean seems to be located systematically farther to the west than that in the observations. Therefore, both the anomalous equatorial easterlies and the off-equatorial wind curls are not as concentrated in the central and the eastern Indian Ocean as are the observed ones. As a result, the model HC anomalies are generated farther west with little space for propagation.

Our results expand the previous studies by Lau and Nath (2000, 2003), which have examined the remote influences of the tropical Pacific on the Indian basin. By prescribing the observed real-time SST in the Pacific Ocean as boundary conditions in an atmospheric GCM with either prescribed climatological SST annual cycle or coupled to a one-dimensional slab ocean model in the Indian Ocean, they have examined the ENSO-induced variability over South Asia as well as the Indian and western Pacific Oceans. Their focus, however, is on the ENSO influences on the Indian and Australian monsoons during the boreal and the austral summer seasons, respectively. A major limitation of Lau and Nath's experiments is that the oceanic dynamics in the Indian Ocean is missing in their experiments and their results are confined to the heat flux influences. Analyzing the same experiments conducted by Lau and Nath (2003), Shinoda et al. (2004) pointed out that the ENSO-induced heat flux fluctuations cannot explain the SST anomalies in the western Indian Ocean. Our present results further demonstrate that the coupled dynamical response within the Indian Ocean associated with the thermocline fluctuation plays an important role in generating the SST fluctuations in the Indian Ocean.

Finally, we would like to emphasize again that the ENSO forcing is not the only way to generate this kind of basinwide Indian Ocean fluctuation. In the second part of this study (Huang and Shukla 2007), a long-term simulation with climatological monthly SST prescribed over the uncoupled oceans will be analyzed and compared with a long-term globally coupled simulation to study the influences of the regional air–sea interactions in a more controlled environment of a suppressed ENSO cycle. The second part of this study shows that the fluctuation of the thermocline depth in the southwestern Indian Ocean can be seen as the regionally dominant mode, even though there is no ENSO signal in this particular run. In this case, the fluctuations of the atmospheric anticyclone over the southern Indian Ocean are partially initiated by the atmospheric disturbances from the northwestern tropical Pacific basin, which trigger the air–sea feedback within the Indian

Ocean. This process seems to share some features described by Annamalai et al. (2003) for observed non-ENSO-related Indian Ocean dipole events, which show precursors in the tropical western Pacific before the anomalous developments start in the Indian Ocean. In the developing stage, the spatial structure of the non-ENSO events is similar to that of the ENSO-related ones. This suggests that the structure of the disturbances is mainly determined by the unstable air–sea feedback on the mean state within the basin. Compared with the non-ENSO events, the unique feature of the ENSO-forced events in the hindcast experiments is that, because of the high persistence of the atmospheric remote forcing from boreal summer to winter, the life span of the thermocline anomalies in the southwestern Indian Ocean is generally longer than that generated by regional coupled processes.

These results suggest that the ENSO influence is to modulate the temporal fluctuation of the Indian Ocean mode through the propagation of the atmospheric planetary waves. The extent of the external influence depends on the amplitude and frequency of the external forcing. As will be shown in the second part of this study, the globally coupled simulation, which produces an ENSO cycle centered at a 5-yr period with weaker amplitude than the observed one, has the interannual variability in the tropical Indian Ocean only weakly linked to the ENSO cycle.

Acknowledgments. This study is supported by a joint grant from the National Science Foundation, the National Oceanic and Atmospheric Administration, and the National Aeronautics and Space Administration. We thank Dr. P. S. Schopf for the development of the Poseidon ocean model, which is used as the oceanic component of the coupled model for this study. We would also like to thank Drs. T. G. Jensen, D. Straus, and two anonymous reviewers for many constructive comments and suggestions for its revision.

REFERENCES

Allan, R., and Coauthors, 2001: Is there an Indian Ocean dipole, and is it independent of the El Niño-Southern Oscillation? *CLIVAR Exchanges,* Vol. 6, No. 3, International CLIVAR Project Office, Southampton, United Kingdom, 18–22.

Annamalai, H., R. Murtugudde, J. Potemra, S. P. Xie, P. Liu, and B. Wang, 2003: Coupled dynamics in the Indian Ocean: Spring initiation of the zonal mode. *Deep-Sea Res. II,* **50,** 2305–2330.

——, P. Liu, and S. P. Xie, 2005: Southwest Indian Ocean SST variability: Its local effect and remote influence on Asian monsoons. *J. Climate,* **18,** 4150–4167.

Bjerknes, J., 1969: Atmospheric teleconnections from the equatorial Pacific. *Mon. Wea. Rev.,* **97,** 163–172.

Black, E., J. Slingo, and K. R. Sperber, 2003: An observational study of the relationship between excessively strong short rains in coastal East Africa and Indian Ocean SST. *Mon. Wea. Rev.,* **131,** 74–94.

Chambers, D. P., B. D. Tapley, and R. H. Stewart, 1999: Anomalous warming in the Indian Ocean coincident with El Niño. *J. Geophys. Res.,* **104,** 3035–3047.

Cheney, R. C., L. Miller, A. Russell, N. Doyle, and J. Lillibridge, 1994: TOPEX/POSEIDON: The 2-cm solution. *J. Geophys. Res.,* **99,** 24 555–24 563.

Clark, C. O., P. J. Webster, and J. E. Cole, 2003: Interdecadal variability of the relationship between the Indian Ocean zonal mode and East African coastal rainfall anomalies. *J. Climate,* **16,** 548–554.

Gualdi, S., E. Guilyardi, P. Delecluse, S. Masina, and A. Navarra, 2003a: The interannual variability in the tropical Indian Ocean as simulated by a CGCM. *Climate Dyn.,* **20,** 567–582.

——, A. Navarra, E. Guilyardi, and P. Delecluse, 2003b: Assessment of the tropical Indo-Pacific climate in the SINTEX CGCM. *Ann. Geophys.,* **46,** 1–26.

Hastenrath, S., 2000: Zonal circulations over the equatorial Indian Ocean. *J. Climate,* **13,** 2746–2756.

——, A. Nicklis, and L. Greischar, 1993: Atmospheric-hydrospheric mechanisms of climate anomalies in the western equatorial Indian Ocean. *J. Geophys. Res.,* **98** (C11), 20 219–20 235.

Hendon, H. H., 2003: Indonesian rainfall variability: Impacts of ENSO and local air–sea interaction. *J. Climate,* **16,** 1775–1790.

Huang, B., 2004: Remotely forced variability in the tropical Atlantic Ocean. *Climate Dyn.,* **23,** 133–152.

——, and J. L. Kinter III, 2000: The interannual variability in the tropical Indian Ocean. Preprints, *10th Conf. on Interaction of the Sea and Atmosphere,* Ft. Lauderdale, FL, Amer. Meteor. Soc., 11–12.

——, and ——, 2001: The interannual variability in the tropical Indian Ocean and its relations to El Niño/Southern Oscillation. COLA Tech. Rep. 94, 48 pp.

——, and ——, 2002: The interannual variability in the tropical Indian Ocean. *J. Geophys. Res.,* **107,** 3199, doi:10:1029/2001JC001278.

——, and J. Shukla, 2007: Mechanisms for the interannual variability in the tropical Indian Ocean. Part II: Regional processes. *J. Climate,* **20,** 2937–2960.

——, P. S. Schopf, and J. Shukla, 2004: Intrinsic ocean–atmosphere variability of the tropical Atlantic Ocean. *J. Climate,* **17,** 2058–2077.

——, J. L. Kinter III, and P. S. Schopf, 2002: Ocean data assimilation using intermittent analyses and continuous model error condition. *Adv. Atmos. Sci.,* **19,** 965–992.

Jury, M. R., and B. Huang, 2004: The Rossby wave as a key mechanism of Indian Ocean climate variability. *Deep-Sea Res. I,* **51,** 2123–2136.

——, D. B. Enfield, and J.-L. Mélice, 2002: Tropical monsoons around Africa: Stability of El Niño–Southern Oscillation associations and links with continental climate. *J. Geophys. Res.,* **107,** 3151, doi:10.1029/2000JC000507.

Kalnay, E., and Coauthors, 1996: The NCEP/NCAR 40-Year Reanalysis Project. *Bull. Amer. Meteor. Soc.,* **77,** 437–471.

Kawamura, R., 1994: A rotated EOF analysis of global sea surface temperature variability with interannual and decadal scales. *J. Phys. Oceangr.,* **24,** 707–715.

Kinter, J. L., III, K. Miyakoda, and S. Yang, 2002: Recent change

in the connection from the Asian monsoon to ENSO. *J. Climate,* **15,** 1203–1215.

Klein, S. A., B. J. Soden, and N.-C. Lau, 1999: Remote sea surface temperature variations during ENSO: Evidence for a tropical atmospheric bridge. *J. Climate,* **12,** 917–932.

Krishnamurthy, V., and B. N. Goswami, 2000: Indian monsoon–ENSO relationship on interdecadal timescale. *J. Climate,* **13,** 579–595.

——, and B. P. Kirtman, 2003: Variability of the Indian Ocean: Relation to monsoon and ENSO. *Quart. J. Roy. Meteor. Soc.,* **129,** 1623–1646.

Lanzante, J. R., 1996: Lag relationships involving tropical sea surface temperatures. *J. Climate,* **9,** 2568–2578.

Lau, N. C., and M. J. Nath, 2000: Impact of ENSO on the variability of the Asian–Australian monsoons as simulated in GCM experiments. *J. Climate,* **13,** 4287–4309.

——, and ——, 2003: Atmosphere–ocean variations in the Indo–Pacific sector during ENSO episodes. *J. Climate,* **16,** 3–20.

Masumoto, Y., and G. Meyers, 1998: Forced Rossby waves in the southern tropical Indian Ocean. *J. Geophys. Res.,* **103,** 27 598–27 602.

Murtugudde, R., R. Seager, and A. Busalacchi, 1999: Interannual variability in the dynamics and thermodynamics of the tropical Indian Ocean. *J. Climate,* **12,** 2300–2326.

——, J. P. McCreary, and A. J. Busalacchi, 2000: Oceanic processes associated with anomalous events in the Indian Ocean with relevance to 1997–1998. *J. Geophys. Res.,* **105,** 3295–3306.

Nicholson, S. E., 1997: An analysis of the ENSO signal in the tropical Atlantic and western Indian Oceans. *Int. J. Climatol.,* **17,** 345–375.

Nigam, S., and H.-S. Shen, 1993: Structure of oceanic and atmospheric low-frequency variability over the tropical Pacific and Indian Oceans. Part I: COADS observations. *J. Climate,* **6,** 657–676.

Pan, Y.-H., and A. Oort, 1990: Correlation analyses between sea surface temperature anomalies in the eastern equatorial Pacific and the world ocean. *Climate Dyn.,* **4,** 191–205.

Parthasarathy, B., and G. B. Pant, 1985: Seasonal relationship between Indian summer monsoon rainfall and Southern Oscillation. *J. Climatol.,* **5,** 369–378.

Rao, S. A., S. K. Behera, Y. Masumoto, and T. Yamagata, 2002: Interannual subsurface variability in the tropical Indian Ocean with a special emphasis on the Indian Ocean dipole. *Deep-Sea Res. II,* **49,** 1549–1572.

Rasmusson, E. M., and T. H. Carpenter, 1983: The relationship between the eastern Pacific sea surface temperature and rainfall over India and Sri Lanka. *Mon. Wea. Rev.,* **111,** 517–528.

Rowell, D. P., 1998: Assessing potential seasonal predictability with an ensemble of multidecadal GCM simulations. *J. Climate,* **11,** 109–120.

——, C. K. Folland, K. Maskell, and M. N. Ward, 1995: Variability of summer rainfall over tropical North Africa (1906–92): Observations and modeling. *Quart. J. Roy. Meteor. Soc.,* **121,** 669–704.

Saji, N. H., B. N. Goswami, P. N. Vinayachandran, and T. Yamagata, 1999: A dipole mode in the tropical Indian Ocean. *Nature,* **401,** 360–363.

Schneider, E. K., B. P. Kirtman, Y. Fan, and Z. Zhu, 2001: Retrospective ENSO forecasts: The effect of ocean resolution. COLA Tech. Rep. 109, 27 pp.

Schopf, P. S., and A. Loughe, 1995: A reduced-gravity isopycnal ocean model: Hindcasts of El Niño. *Mon. Wea. Rev.,* **123,** 2839–2863.

Shinoda, T., M. A. Alexander, and H. H. Hendon, 2004: Remote response of the Indian Ocean to interannual SST variations in the tropical Pacific. *J. Climate,* **17,** 362–372.

Shukla, J., 1987: Interannual variability of monsoons. *Monsoons,* J. S. Fein and P. L. Stephens, Eds., John Wiley & Sons, 399–463.

——, and D. A. Paolino, 1983: The Southern Oscillation and long-range forecasting of the summer monsoon rainfall over India. *Mon. Wea. Rev.,* **111,** 1830–1837.

Smith, T. M., R. W. Reynolds, R. E. Livezey, and D. C. Stokes, 1996: Reconstruction of historical sea surface temperatures using empirical orthogonal functions. *J. Climate,* **9,** 1403–1420.

Tourre, Y. M., and W. B. White, 1995: ENSO signals in global upper-ocean temperature. *J. Phys. Oceangr.,* **25,** 1317–1332.

Venzke, S., M. Latif, and A. Villwock, 2000: The coupled GCM ECHO-2. Part II: Indian Ocean response to ENSO. *J. Climate,* **13,** 1371–1383.

Wang, B., R. Wu, and T. Li, 2003: Atmosphere–warm ocean interaction and its impacts on Asian–Australian monsoon variation. *J. Climate,* **16,** 1195–1211.

Webster, P. J., and S. Yang, 1992: Monsoon and ENSO: Selectively interactive systems. *Quart. J. Roy. Meteor. Soc.,* **118,** 877–926.

——, V. O. Magaña, T. N. Palmer, R. A. Thomas, M. Yanai, and T. Yasunari, 1998: Monsoons: Processes, predictability, and the prospects for prediction. *J. Geophys. Res.,* **103,** 14 451–14 510.

——, A. M. Moore, J. P. Loschnigg, and R. R. Leben, 1999: Coupled ocean–atmosphere dynamics in the Indian Ocean during 1997–98. *Nature,* **401,** 356–360.

Xie, S.-P., H. Annamalai, F. A. Schott, and J. P. McCreary Jr., 2002: Structure and mechanisms of south Indian Ocean climate variability. *J. Climate,* **15,** 864–878.

Yu, L., and M. M. Rienecker, 1999: Mechanisms for the Indian Ocean warming during the 1997–1998 El Niño. *Geophys. Res. Lett.,* **26,** 735–738.

Zhang, R., A. Sumi, and M. Kimoto, 1999: A diagnostic study of the impact of El Niño on the precipitation in China. *Adv. Atmos. Sci.,* **16,** 229–241.